FEATURE-BASED MESH ADAPTATION APPLIED TO THE LARGE-EDDY SIMULATION OF MULTIPLE JETS IMPINGING ON A SURFACE

A. Grenouilloux[1,2,*], V. Moureau[1], G. Lartigue[1], P. Bénard[1], P. Ferrey[2]

[1]CORIA, CNRS UMR6614, Normandie Universite, UNIROUEN, INSA of Rouen,France
[2]Safran Nacelles, Route du Pont VIII BP 91, Gonfreville-l'Orcher, 76700, France

ABSTRACT

In the context of the prediction of convective heat transfers in turbulent fluids, a novel methodology for the featured-based mesh adaptation of unstructured grids is proposed. This approach, which relies on Large-Eddy Simulation (LES), proposes to refine and coarsen cells according to the local dissipation of the overall kinetic energy [1]. This adaptation criterion is supplemented with a set of user-defined constraints such as the minimum and maximum cell size, the metric gradient, the final number of elements in the adapted grid [2] and importantly, the non-dimensional wall unit y^+ on boundaries where heat transfer occurs. The statistical convergence of the dissipation of the kinetic energy is assessed thanks to a time series analysis at several probe locations. The methodology is validated for a row of multiple jets impinging on a flat surface at a Reynolds number $Re = 23\,000$ and a nozzle to plate distance $H/D = 5$ [3]. The proposed adaptation strategy is general and has been designed to be applied to any complex aerothermal industrial configuration.

1 INTRODUCTION

Jet impingement is widely used in industrial applications to locally increase heat exchange. Its design is crucial so that components operating in extreme conditions can withstand high thermal loads. In impinging configurations, heat transfer is driven by the interactions of large and small eddies with the exchanging surfaces, which need to be properly resolved or modeled to predict global performances. For the past decades, Reynolds Averaged Navier-Stokes (RANS) simulations have tried to predict the aerothermal response in these configurations, but the presence of two different flow regions before and after impingement has often led to inaccurate results [4]. Large-Eddy Simulation (LES) has become a valuable tool for the simulation of turbulent and unsteady flows. This numerical method is based on a scale separation obtained by filtering the Navier-Stokes equations: the large scales are solved explicitly while the smallest ones are modelled. The cutoff wave number has to be in the inertial range to guarantee that the role of modeled scales is limited to diffusing the resolved scales through sub-grid turbulent transport. In most LES solvers, the filtering is implicit and directly linked to the local cell size. Thus, the mesh resolution has a major impact on the solution quality: a fine grid must be used in regions with high turbulent intensity. A considerable amount of time is often spent by users in the design of a suitable, yet user-dependent mesh.

Recent developments in mesh adaptation have allowed to target specific features to improve results [2, 1, 5]. In the present paper, a methodology for the feature-based mesh adaptation based on the dissipation of the kinetic energy (KE) combined with specific near-wall refinement is presented. A row of three jets impinging on a flat surface at a nozzle-to-plate distance $H/D = 5$ and a Reynolds number $Re = 23\,000$ [3] is considered for validation. In the first section, the methodology for the mesh adaptation is presented. Then, the row of impinging jets is studied under two configurations, namely confined and unconfined flow conditions. Results obtained with the present approach are compared with the available experimental data [3].

*Corresponding author: adrien.grenouilloux@coria.fr

2 ADAPTATION METHODOLOGY

In this section, the quantity of interest for mesh adaptation is presented. The mesh adaptation procedure is then exposed, with a particular emphasis on the assessment of the time convergence of quantities of interest.

2.1 Mesh adaptation criteria

In Benard et al. [2], two criteria for mesh adaptation are presented: the first one, called Qc_1, aimed at decreasing the interpolation error thanks to a Hessian-based error estimator and the second one, called Qc_2 or Pope's criterion, ensured the resolution of a least 80% of the total turbulent-kinetic energy (TKE) spectrum [6] in order to guarantee that the LES cutoff scale is in the inertial range of the TKE spectrum. Recently, Daviller et.al [1] proposed a method for the mesh adaptation of swirl flows based on the overall dissipation of the kinetic energy. Indeed, the so-called LIKE criterion allows to refine complex geometries to match the correct pressure loss, such as in an injector [1]. In this formulation, no control of the final cell count is presented. Hence, the proposed methodology can lead to very large meshes that are not compatible with the user's computational resources. It is therefore proposed to extend the work of Benard et al. [2] with a new mesh adaptation criterion Qc_3:

$$Qc_3 = \Delta^2 \;\; 2(\nu + \nu_t)\overline{S}_{ij} \;\; \overline{S}_{ij}\,. \tag{1}$$

Here Δ and $\overline{S}_{ij}$ account for the local cell size and the symmetric part of the strain tensor based on the filtered velocity, respectively. Therefore the quantity Qc_3 represents the overall dissipation of the kinetic energy (KE) weighted by the square of the local cell size. This latter allows to compute a local refinement ratio τ_{QC3} and to impose constraints on the final grid as for Qc_1 and Qc_2 [2].
To improve aerothermal results in the near wall region, an additional criterion is also considered. The resolution of the near-wall boundary layer can be assessed by the non-dimensional cell size given in wall units $y^+ = \frac{u_\tau \Delta}{\nu}$, where u_τ represents the friction velocity. The friction velocity depends on the velocity gradient at the wall and is therefore hard to estimate on coarse grids. This problem is circumvented in Grenouilloux et al. [7], where an analytical wall law (WL) is used to avoid computing the wall velocity gradient. This method relies on the use of the local product u^+y^+, which is equivalent to a Reynolds number based on the cell size at the wall and the tangential velocity at this distance, to compute an accurate value of y^+_{WL}. Here, the considered analytical wall-law profile is the one of Duprat et al. [8]. An accurate estimation of the near-wall refinement ratio τ_{y^+} is then deduced from y^+_{WL} and from the target value.

2.2 Statistical convergence

Assessing the convergence of a statistical estimator for a stochastic variable, especially in highly turbulent regions, is not straightforward. However, building an adapted mesh on data which is not statistically converged can lead to erroneous cell size and refinement ratio. Therefore, a method based on the work of [9] is developed in the present study to guarantee a given level of convergence for the time average and the root mean square (RMS) of Qc_3 in regions of interest. This method relies on a set of probes located in the most relevant regions which sample the instantaneous values of $Qc_3(t)$ at every iteration. During the simulation, the sampled time series is then subdivided into disjoint intervals by a binary tree procedure [10]. The statistical estimators are then computed on every independent interval and compared with each others. When the variation of an estimator on the coarsest levels falls below a given threshold, the associated quantity (average or RMS) is supposed to be statistically converged. The global convergence is thus reached only when all the probes are converged.

2.3 Mesh adaptation algorithm

The iterative mesh convergence process consists of a succession of simulations for statistical convergence and a series of mesh adaptation steps. The simulation is continued until the statistical convergence of Qc_3 (both average and RMS) is achieved, as explained in section 2.2. Then, a refinement ratio τ_{QC3} based on the time average of the dissipation of the kinetic energy $\langle Qc_3 \rangle_t$ is computed. A series of constraints are then applied to τ_{QC3} in order to respect a set of user-defined parameters, such as a minimal h_{min} and maximal h_{max} cell size, a metric gradient h_{grad} to ensure the correct transition from coarse to fine cells, and a targeted number of elements on the adapted grid $N_{elem,target}$ [2]. On top of that, a characteristic near wall refinement τ_{y+} based on the equivalent non-dimensional wall unit y^+_{WL} is applied on the impinging plate to impose a minimal value of y^+ as described in section 2.1. The process is repeated until the adapted grid respects all the user-defined constraints.

3 VALIDATION TEST CASE: ROW OF IMPINGING JETS

The iterative process for mesh convergence presented in section 2.3 is applied to a row of impinging jets in two configurations, namely confined and unconfined [3]. First, the test case and the numerical set-up are recalled. Then, the mesh obtained with the procedure introduced in section 2 is presented and compared with the initial grid. Finally, an overview of the heat-transfer data is given for the unconfined case.

3.1 Geometry and numerical set-up

A row of three jets impinging on a flat surface at a Reynolds number $Re = 23\,000$ and a nozzle to plate distance $H/D = 5$ is considered. As depicted by Fig. 1, the numerical domain consists of a $27D \times 36D \times 5D$ box, with three cylindrical inlets of diameter D as described in [3] .

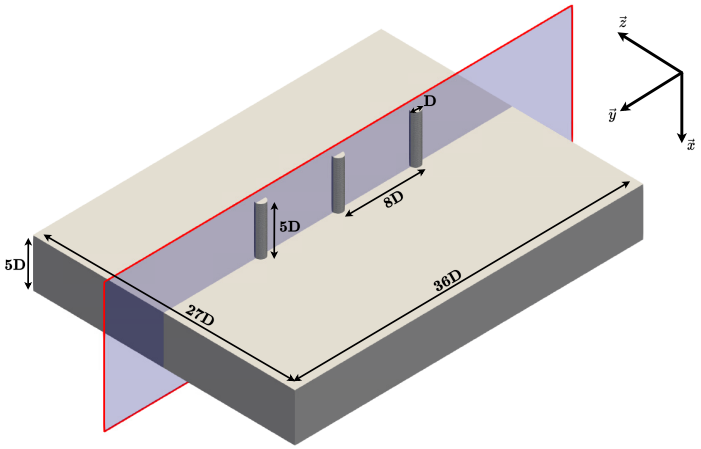

Figure 1: Overview of the numerical domain with the normal plane to the $\vec{z}$ axis used for the data display.

The velocity profile presented in [11] is imposed on the three inlets:

$$\frac{U(r)}{U_c} = \alpha \left(1 - \frac{2r}{D}\right)^{1/7.23}, \tag{2}$$

with a centerline velocity U_c derived from the bulk velocity as $U_b/U_c = 0.811 + 0.038(\log(Re_b) - 4)$. A rescaling coefficient α is used to guarantee the correct velocity flowrate across every inlet. To trigger the development of the turbulence inside the pipe, homogeneous isotropic turbulence (HIT) based on a Passot-Pouquet spectrum [12] is injected. The latter is parametrized by a characteristic length $L_e = D/3$ and a turbulence intensity of $TI = 5\%$. Two main configurations are considered for validation, namely

a confined (CO) and an unconfined cases (UNCO). In the former, the upper plate is considered as an adiabatic no-slip wall while in the latter, the upper boundary is considered as an inlet with a constant velocity equal to 5% of the bulk velocity. The four lateral boundaries are considered as outlets. The WALE turbulence model [13] is used for both configurations. All the simulations are performed with the unstructured low-Mach number code YALES2 [14] featuring parallel dynamic mesh adaptation [2] with the MMG3D library. The time integration relies on the fourth-order accurate TFV4A scheme [15] and the spatial discretization on a fourth-order accurate central finite-volume scheme [16].
The reduced temperature $\overline{\theta} = (\overline{T} - T_\infty)/(T_w - T_\infty)$ is defined from the temperature T, the temperature of the bottom plate $T_w = 330$K and the freestream temperature $T_\infty = 300$K [11]. This variable is solved with the following equation:

$$\frac{\partial \overline{\theta}}{\partial t} + \nabla \cdot (\overline{u}\overline{\theta}) = \nabla \cdot (D_\theta \nabla \cdot \overline{\theta}). \tag{3}$$

Here D_θ represents the overall diffusivity and is therefore the sum of the molecular and turbulent diffusivities. These parameters are respectively defined from the laminar Prandtl number $Pr_{air} = 0.71$, and the turbulent Prandtl number $Pr_{t,air} = 0.9$. Following the approach of [11], Dirichlet boundary conditions are imposed at the three jet inlets ($\overline{\theta} = 0$) and on the bottom plate ($\overline{\theta} = 1$). Regarding the upper plate, an adiabatic condition is imposed in the confined configuration and a Dirichlet condition ($\overline{\theta} = 0$) is used in the unconfined case.

3.2 Grid convergence

An initial mesh (MI) of 17.5M cells is used for both cases (see Fig. 2 Top). This coarse grid has a global cell size of 2.5 mm with finer cells of 1 mm near walls. The mesh adaptation strategy presented in section 2.3 is applied with the following constraints for the metric field. First, the refinement ratio τ_{QC3} is truncated so that the maximum cell size allowed in the domain is $h_{max} = 5$ mm, and the minimum cell size allowed is $h_{min} = 10\mu$m. Then, to ensure a smooth transition between fine and coarse regions, the metric gradient is limited to $h_{grad} = 0.3$, i.e. a 30% maximum increase in size for two neighbor cells. The near wall refinement ratio τ_{y^+} is set so that $y^+_{WL} \approx 10$ on the impinging plate. Finally, the targeted number of elements for the final grid is $N_{elem,target} = 200$M.

The initial and final grid sizes for both cases are summarised in Tab. 1. An overview of the final grid for the unconfined case (MF-UNCO) is presented in Fig. 2. The grid obtained for the confined case is very similar to the one obtained for the unconfined case and is therefore not presented here. Note that a tolerance of up to 5% for the final number of elements is accepted to account for the possible interpolation errors of the metric field.

Table 1: Computation cases

Case	Initial mesh (MI)	Final mesh (MF)
Confined (CO)	17.5 M	191 M
Unconfined (UNCO)	17.5 M	196 M

3.3 Aerothermal results

The methodology presented above is able to successfully refine the key regions for this configuration. More precisely, the quantity Qc_3 is able to detect the shear layer at the nozzle exit, where Kelvin-Helmholtz structures arise and develop. These primary and large scale structures have been reported in the literature as the main drivers of the heat-transfer mechanism along the impinging plate [17, 11]. The dead-flow regions are also detected as low-interest zones and the mesh is coarsened there. Moreover, the refinement of the pipe walls ensured the correct development of turbulence before exiting the nozzle.

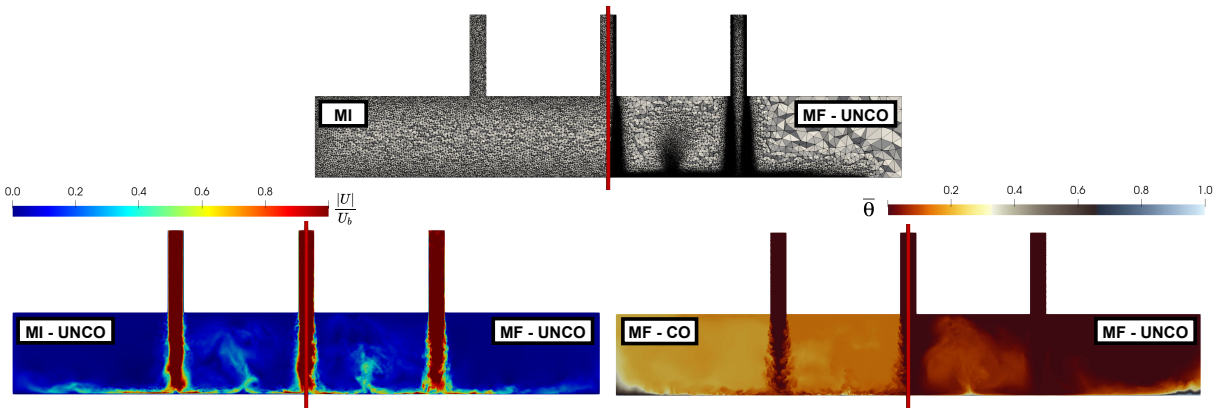

Figure 2: Top: Overview of the grids. The red line separates the initial mesh (MI) from the final mesh for the unconfined test case (MF-UNCO). Bottom-Left: Overview of the instantaneous velocity of the unconfined case (UNCO). The red line separates the results on the initial mesh (MI) and on the final mesh (MF). Bottom-Right: Overview of the instantaneous dimensionless temperature $\overline{\theta}$ on the final grids. The red line separated the confined case (CO) from the unconfined case (UNCO).

The confinement plate has a major impact on the temperature field, as it can be noticed in Fig. 2: it enables the presence of strong recirculation zones that homogenize the temperature in the domain.

The heat-transfer coefficients on the impinging plate are validated against the experimental data of Fénot et al. [3]. The Nusselt number Nu is computed from the temperature flux that is imposed on the impinging plate to ensure the Dirichlet condition $\overline{\theta} = 1$ [18]. This latter approach ensures a better estimation of the local heat-transfer coefficient than the direct use of the temperature gradient $\nabla\overline{\theta}$, especially on the initial coarse grid (MI). The influence of turbulent structures on the instantaneous Nusselt number can be seen in Fig. 3 (Left). A comparison between the numerical and the experimental average Nusselt number is presented in Fig. 3 (Center). Some minor differences with experimental results still arise on the Nusselt number distribution: a possible explanation is that the conduction inside the impinging plate is not taken into account in the present simulation. Even not shown here, a good agreement for the confined case (CO) on the final grid (MF) is found as well. Figure 3 (Right) shows that the targeted value $y^+_{WL} = 10$ is almost reached on the final grid with $6 < y^+_{WL} < 12$.

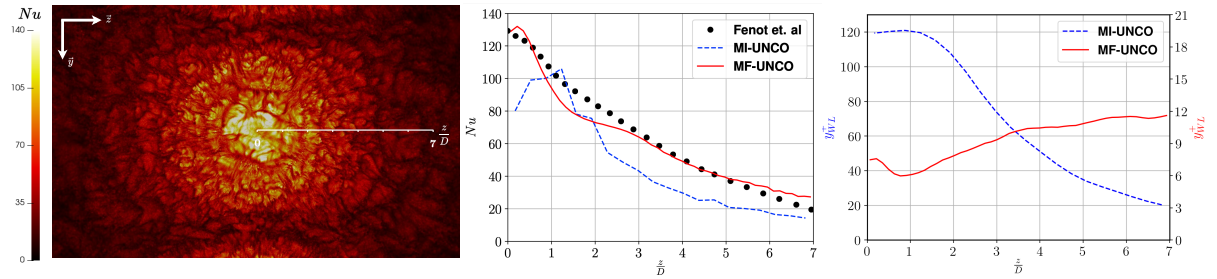

Figure 3: Left: Close view of the instantaneous Nusselt number Nu on the final grid for the unconfined case (UNCO). Center: Nusselt number distribution for the central jet along the $\vec{z}$ direction. Right: y^+_{WL} distribution for the central jet along the $\vec{z}$ direction.

4 CONCLUSION AND PERPECTIVES

A novel methodology to achieve both mesh and statistical convergence of aerothermal simulations has been presented. Based on a the work of Benard et al. [2] and Daviller et al. [1], a new refinement

criterion Qc_3 computed from the dissipation of the kinetic energy has been used to adapt the grid. This methodology allows to control key parameters on the final grid, such as the minimum h_{min} and maximum h_{max} cell size, a metric gradient h_{grad} and the final number of elements $N_{elem,target}$. A near-wall refinement τ_{y^+} is added as a constraint to impose values of the non-dimensional wall unit y^+_{WL} based on the wall law of Duprat et al. [8] in order to improve the prediction of heat transfer. The whole methodology is applied to a row of jets impinging on a surface under two configurations, namely confined and unconfined. The numerical results for both cases are in good agreement with the experimental data of Fénot et al. [3]. A dedicated methodology, based on a binary tree decomposition of the instantaneous $Qc_3(t)$ time signal of appropriate probes, is used to ensure the statistical convergence of the refinement criterion in capital areas as the shear layer and the impinging region.
For future work, the present methodology will be extended to even more complex configurations and will be coupled to anisotropic mesh refinement to improve the time-to-solution cost.

ACKNOWLEDGEMENTS

This work is granted access to the HPC resources of CINES/TGCC under the projects 2B06880 and made by GENCI and of CRIANN under the allocation 2012006.

REFERENCES

[1] G. Daviller, M. Brebion, P. Xavier, G. Staffelbach, J.-D. Müller, & T. Poinsot. A Mesh Adaptation Strategy to Predict Pressure Losses in LES of Swirled Flows. *Flow, Turbulence and Combustion*, **99** (2017) 93–118.

[2] P. Benard, G. Balarac, V. Moureau, C. Dobrzynski, G. Lartigue, & Y. D'Angelo. Mesh adaptation for large-eddy simulations in complex geometries. *International Journal for Numerical Methods in Fluids*, **81** (2016) 719–740.

[3] M. Fenot, J.-J. Vullierme, & E. Dorignac. Local heat transfer due to several configurations of circular air jets impinging on a flat plate with and without semi-confinement. *International Journal of Thermal Sciences*, **44** (2005) 665–675.

[4] N. Zuckerman & N. Lior. Jet Impingement Heat Transfer: Physics, Correlations, and Numerical Modeling. volume 39 of *Advances in Heat Transfer*, pp. 565–631. Elsevier (2006).

[5] P. W. Agostinelli, B. Rochette, D. Laera, J. Dombard, B. Cuenot, & L. Gicquel. Static mesh adaptation for reliable large eddy simulation of turbulent reacting flows. *Physics of Fluids*, **33** (2021) 035141.

[6] S. B. Pope. *Turbulent Flows*. Cambridge University Press (2000).

[7] A. Grenouilloux, G. Balarac, & J. Leparoux. On the use of kinetic-energy balance for the feature-based mesh adaptation applied to Large-Eddy Simulation in complex geometries. ASME (2022).

[8] C. Duprat, G. Balarac, O. Metais, P. Congedo, & O. Brugiere. A wall-layer model for large-eddy simulations of turbulent flows with/out pressure gradient. *Physics of Fluids - PHYS FLUIDS*, **23**.

[9] M. Papageorge & J. Sutton. Statistical processing and convergence of finite-record-length time-series measurements from turbulent flows. *Experiments in Fluids*, **57**.

[10] M. Wallerberger. Efficient estimation of autocorrelation spectra. *arXiv: Computational Physics*.

[11] P. Aillaud, F. Duchaine, L. Y. M. Gicquel, & S. Didorally. Secondary peak in the Nusselt number distribution of impinging jet flows: A phenomenological analysis. *Physics of Fluids*, **28** (2016) 095110.

[12] H. Boughanem. Validation du code de simulation directe ntmix3d pour le calcul des ecoulements turbulents reactif. Technical report, IFP (1996).

[13] N. Franck & F. Ducros. Subgrid-Scale Stress Modelling Based on the Square of the Velocity Gradient Tensor. *Flow Turbulence and Combustion*, **62** (1999) 183–200.

[14] V. Moureau, P. Domingo, & L. Vervisch. Design of a massively parallel CFD code for complex geometries. *Comptes Rendus Mécanique*, **339** (2011) 141–148. High Performance Computing.

[15] M. Kraushaar. *Application of the compressible and low-mach number approaches to large eddy simulation of turbulent flows in aero-engines*. Ph.D. thesis, INPT (2011).

[16] M. Bernard, G. Lartigue, G. Balarac, V. Moureau, & G. Puigt. A framework to perform high-order deconvolution for finite-volume method on simplicial meshes. *International Journal for Numerical Methods in Fluids*, **92** (2020) 1551–1583.

[17] O. Neumann, N. Uddin, & B. Weigand. *Grid Sensitivity of LES Heat Transfer Results of a Turbulent Round Impinging Jet*, pp. 307–325 (2011).

[18] P. Benard. *Analyse et amélioration d'une chambre de combustion centimétrique par simulations aux grandes échelles*. Theses, INSA de Rouen (2015).